

Underwater acoustic properties of graphene nanoplatelet-modified rubber

Baihua Yuan¹, Weikang Jiang¹, Heng Jiang², Meng Chen² and Yu Liu²

Journal of Reinforced Plastics and Composites
2018, Vol. 37(9) 609–616
© The Author(s) 2018
Reprints and permissions:
sagepub.co.uk/journalsPermissions.nav
DOI: 10.1177/0731684418754411
journals.sagepub.com/home/jrp


Abstract

A series of graphene nanoplatelet-modified acrylonitrile-butadiene rubber-based underwater acoustic absorbing materials were prepared. The dynamic mechanical properties, underwater sound absorption properties, differential scanning calorimetry, vulcanization property, and mechanical properties of graphene nanoplatelets/acrylonitrile-butadiene rubber nanocomposites were studied theoretically and experimentally. The results indicated that graphene nanoplatelet-modified acrylonitrile-butadiene rubber-based underwater acoustic absorbing materials exhibited excellent damping and underwater sound absorption properties. The storage modulus (E') and loss modulus (E'') of graphene nanoplatelets/acrylonitrile-butadiene rubber nanocomposites were increased significantly with increasing graphene nanoplatelets content. At a graphene nanoplatelets content of 25 phr, the E' and E'' at 15°C improved by 1201 and 603%, respectively. The obvious improvement in E' and E'' were mainly attributed to the extremely high interfacial contact area between graphene nanoplatelets and acrylonitrile-butadiene rubber chains and the ultrahigh mechanical properties of graphene nanoplatelets. The underwater sound absorption coefficient (α) was increased obviously as the graphene nanoplatelets were incorporated. The optimal α of the nanocomposites was achieved as the graphene nanoplatelets content was 10 phr, and the average value of α was improved from 0.35 to 0.73—an increase of nearly onefold. The notable improvement in α was due to the marked increase in damping properties and thermal conductivity of graphene nanoplatelets/acrylonitrile-butadiene rubber nanocomposites. The merits of graphene nanoplatelet-modified underwater acoustic absorbing materials were higher damping, better underwater sound absorption, and better mechanical properties with unaffected density in comparison to other inorganic and rigid fillers or porous fillers.

Keywords

Graphene nanoplatelet-modified, underwater acoustic absorbing materials, underwater acoustic properties

Introduction

Underwater acoustic absorbing materials are often placed on the surface of submarine to prevent detection by active sonar.^{1,2} To reduce the sonar echo, the acoustic absorbing material must meet the following two conditions^{1,3,4}: The impedance should match seawater as much as possible so that the incident sound wave can enter into the material interior without being reflected; second, the material should have excellent ability to attenuate and disperse sound wave so that the incoming sound wave can be converted into heat energy.

Rubber is usually selected as the matrix of the acoustic absorbing material due to its impedance matching and high damping ability. However, the sound absorption properties of pure rubber matrix are not satisfactory for practical applications unless

they are improved by introducing inorganic and rigid fillers (e.g. graphite, mica powder, etc.) or porous fillers (e.g. vermiculite powder, hollow glass, aluminum microspheres, etc.) into the matrix.³ Generally, it is necessary to add a large amount of such fillers into the matrix to obtain the desired acoustic absorbing

¹Institute of Vibration, Shock and Noise, School of Mechanical Engineering, Shanghai Jiaotong University, Shanghai, People's Republic of China

²Key Laboratory of Microgravity, Institute of Mechanics, Chinese Academy of Sciences, Beijing, People's Republic of China

Corresponding author:

Weikang Jiang, Department of Engineering Mechanics, Minhang, Shanghai 200240, People's Republic of China.

Email: wkjiang@sjtu.edu.cn

properties, but this results in a sharp decrease in mechanical properties and a significant increase in density.

Recently, graphene nanoplatelets (GnPs) and their derivatives such as graphene oxide (GO)-modified nanocomposites have attracted tremendous attention due to their ultrahigh mechanical properties. The Young's modulus and intrinsic strength of single graphene sheet are 1 TPa and 130 GPa,⁵ respectively. They have a high specific surface area ($\sim 2630 \text{ m}^2/\text{g}^6$) as well as high thermal and electronic conductivity ($\sim 5000 \text{ W}/(\text{m} \cdot \text{K})$ and $2 \times 10^4 \text{ cm}^2/(\text{V} \cdot \text{S})$,⁷⁻⁹ respectively). They also have good barrier properties.⁸⁻¹⁰ These unique properties not only significantly improve the mechanical properties of the modified nanocomposites, but also remarkably increase the functional properties such as thermal and electronic conductivity, damping, and barrier properties. Many works have been focused on the preparation and functionalization of graphene and its derivatives,¹¹⁻¹⁷ the preparation of graphene-based nanocomposites, the improvements in mechanical or dynamic mechanical properties, thermal and electronic conductivity, and barrier properties.¹⁸⁻²⁶ However, there are no reports on the underwater acoustic properties of GnP-modified nanocomposites.

In this study, a series of GnP-modified acrylonitrile-butadiene rubber-based (NBR-based) underwater acoustic absorbing materials were prepared by mechanical mixing method. The effects of GnPs content on the dynamic mechanical properties, underwater sound absorption properties, differential scanning calorimetry (DSC), vulcanization property, mechanical properties, as well as SEM micrographs of the GnPs/NBR nanocomposites were investigated theoretically and experimentally. The sound absorption mechanisms of the GnPs/NBR nanocomposites were explored theoretically. The merits of the GnP-modified acoustic absorbing materials were discussed and compared with other

traditional inorganic and rigid fillers and porous fillers modified acoustic absorbing materials.

Experimental

Materials

NBR DN4050 was supplied by Zeon Chemicals L.P. The average Mooney viscosity ML (1 + 4) of this solid rubber was 47 at 100°C, and the content of bound acrylonitrile was 40%. The GnPs (type of SE 1430) were obtained from The Sixth Element (Changzhou) Materials Technology Co., Ltd. The average diameter, bulk density, thickness, and surface area of the GnPs was 7 μm , 0.05 g/cm^3 , 50–65 nm, and 206 m^2/g , respectively. Carbon black (N330) was supplied by Cabot Corporation. The colloidal graphite powder with the particle diameter of 325 mesh was supplied by Qingdao Tianhe Graphite Co., Ltd. Stearic acid was purchased from Hangzhou Oleochemicals Co., Ltd. The curing agent was insoluble sulfur, and the curing activator was nanometer zinc oxide (ZnO), which is vulcanization accelerator. The *N*-cyclohexylbenzothiazole-2-sulphenamide (CZ) and tetramethylthiuram disulfide (TMTD) were supplied by Lanxess Energizing Chemistry Corporation.

Preparation of GnPs/NBR nanocomposites

The samples were compounded with different concentrations of GnPs according to Table 1. The equipment and procedures for preparation, mixing, and vulcanization were in accordance with International Standard ISO 2393:2014(E). The most critical equipment for the preparation was an internal mixer with type of GE 5 and with an intermeshing rotor. The total volume, fill factor, and rotor speed of the internal mixer was 5L, 0.65, and 20–100 r/min, respectively. In order to obtain

Table 1. Formulation of GnP-filled NBR systems.

Ingredients (phr)	Formula no.					
	SMX-001	SMX-002	SMX-003	SMX-004	SMX-005	SMX-006
NBR DN4050	100	100	100	100	100	100
ZnO	5	5	5	5	5	5
Stearic acid	1	1	1	1	1	1
Carbon black N330	30	30	30	30	30	30
GnPs	0	5	10	15	20	25
Colloidal graphite powder	20	20	20	20	20	20
Insoluble sulfur	1.5	1.5	1.5	1.5	1.5	1.5
CZ	1.5	1.5	1.5	1.5	1.5	1.5
TMTD	0.3	0.3	0.3	0.3	0.3	0.3

CZ: *N*-cyclohexylbenzothiazole-2-sulphenamide; GnP: graphene nanoplatelet; NBR: butadiene-acrylonitrile rubber; TMTD: tetramethylthiuram disulfide; ZnO: zinc oxide.

the identical degree of GnPs dispersion of each sample, it was important to keep the process parameters of each sample strictly consistent. The main process parameters were as follows: (1) The rubber compounding was done in two stages. In the first stage, rubber was mixed with ZnO, stearic acid, GnPs, carbon black, and colloidal graphite powder in an internal mixer. The internal mixer rotor speed and the cooling water temperature were 20 r/min and $15 \pm 2^\circ\text{C}$. All fillers were added over 2–3 min, and the mixing was further proceeded for another 5 min until the temperature of the rubber compound reached 110°C . The compound was then discharged from the mixer. (2) In the second stage the curing agent and vulcanization accelerator were added to compound using a mixing mill. The clearance between rolls of mixing mill was 0.5 mm, the cooling water temperature was $15 \pm 2^\circ\text{C}$, and the compound was processed for 15 min. (3) The vulcanization process performed by compression molding process at 150°C for 50 min under 10 MPa pressure for the specimens testing underwater sound absorption properties ($\Phi 57\text{ mm} \times 40\text{ mm}$) and at 160°C for 10 min under 10 MPa pressure for the other test specimens ($200\text{ mm} \times 200\text{ mm} \times 2\text{ mm}$).

Characterization

Dynamic mechanical analysis (DMA). The DMA was carried out on a DMA +100 analyzer (01dB-Metravib, France) with a tensile mode over a temperature range from -30°C to $+60^\circ\text{C}$ at a heating rate of $3^\circ\text{C}/\text{min}$ at 10 Hz. The specimen was a rectangular strip ($40\text{ mm} \times 10\text{ mm} \times 2\text{ mm}$). The tests were performed according to ASTM D 5026-2015. The storage modulus (E') and loss modulus (E'') were evaluated.

Underwater sound absorption properties. The underwater sound absorption properties were carried out on a $\Phi 57\text{ mm}$ pulse tube and corresponding equipment shown in Figure 1 according to GB/T 14369-2011. The sample ($\Phi 57\text{ mm} \times 40\text{ mm}$) was bonded on a 10 mm thick stainless steel column and placed in the end of the pulse tube. The nozzle of the tube was filled with nitrogen as a reflector so that the transmitted sound waves can be reflected back completely and be detected as a reflected signal (R) by the transducer placed in the bottle of the tube. The sound absorption coefficient (α) was then calculated by $\alpha = 1 - |R|^2$. The frequency was from 2 to 30 kHz, and the water temperature was 15°C . The hydrostatic pressure was 0.1 MPa. Every sample was soaked in water for 24 h before testing.

DSC. The DSC tests were performed on a DSC apparatus of Mettler Toledo (model: DSC1) (produced by Mettler-Toledo, Switzerland) at a heating rate of

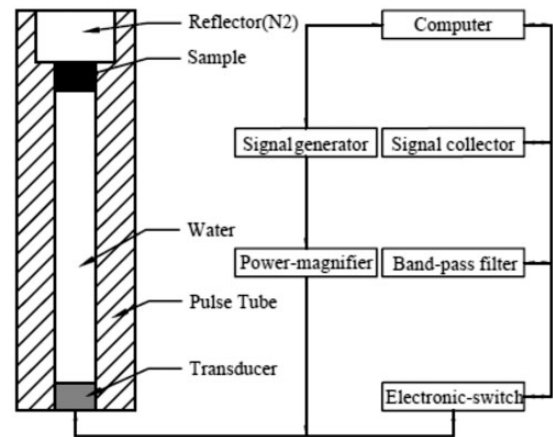


Figure 1. Test set for the underwater acoustic properties (Ref. GB/T 14369-11).

$10^\circ\text{C}/\text{min}$ from -70 to 155°C under a nitrogen atmosphere. The glass transition temperature (T_g) values have been deduced from the inflection point of the DSC curves on the heating run.

Vulcanization property. Vulcanization property of the GnPs/NBR nanocomposites was carried out on a rotorless cure meters (type GT-M2000A, GOTECH testing Machines Inc.) according to ASTM D5289-2007a. The test temperature was 160°C , and the amplitude of the oscillation was $\pm 0.5^\circ$.

Mechanical properties. Tensile and tear properties were performed using a computer controlled electronic universal testing machine RGM-3030 (Shenzhen Reger Instrument Co., Ltd, China) according to ASTM D412-06a (reapproved 2013) and ASTM D624-00 (reapproved 2012), respectively. The rates of grip separation for tensile and tears tests were 500 mm/min. The durometer hardness was tested using a type A durometer according to ASTM D 2240-15.

Results and discussions

DMA

Figures 2 and 3 show the temperature dependence of the storage modulus (E') and the loss modulus (E'') when the content of GnPs was 0, 5, 10, and 25 phr, respectively. The peak of the E'' curve corresponds to the glass transition temperature (T_g) of the nanocomposite. The E' and E'' were significantly improved with increasing GnPs content both in the glassy state and in the rubbery plateau region. When the GnPs content was 5 phr, the E' and E'' at 15°C were improved by 94 and 84%, respectively. When the GnPs content increased to 25 phr, the E' and E'' at 15°C were

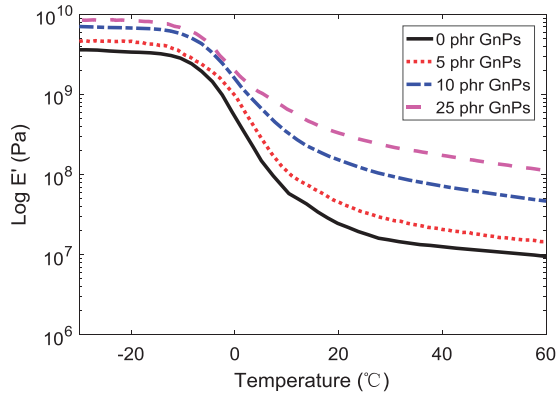


Figure 2. The temperature dependency of the E' . GnP: graphene nanoplatelet.

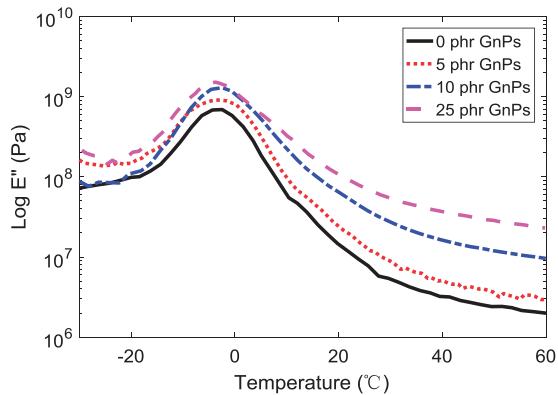


Figure 3. The temperature dependency of the E'' . GnP: graphene nanoplatelet.

improved by 1201 and 603%, respectively. While the T_g was unaffected, the temperature range of glass–rubber transition region was markedly widened. This indicates that the incorporation of GnPs can not only greatly improve the stiffness of the polymer matrix, but can also significantly increase the damping properties and broaden the damping temperature and frequency limits of the matrix.

There are two mechanisms that account for this obvious improvement in E' . First, the interface bonding strength of GnPs and NBR matrix was greatly reinforced due to the high specific surface area of GnPs. This results in an efficient transformation of stress from the matrix to GnPs.¹⁹ Second, since the elastic modulus of GnPs is much higher than the modulus of NBR matrix, this introduces and distributes a large amount of spring with a higher elastic modulus in the NRB matrix in parallel. Thus, the elastic modulus of the composite system was dramatically improved. Obviously, E' increases as more GnPs are incorporated.²⁷

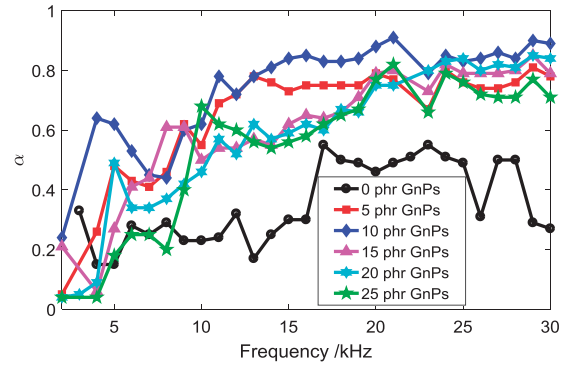


Figure 4. The underwater sound absorption coefficient spectra of nanocomposites with different GnPs contents. GnP: graphene nanoplatelet.

There are two main mechanisms on how to increase the E'' . First, when GnPs were incorporated, the free volume portion of NBR matrix was filled partly by GnPs. This enhanced the degree and number of entanglements between molecular chains of the matrix, the viscosity of the composite system, the internal friction between the GnPs and polymer chains, as well as friction between GnPs. In addition, the interfacial contact area between the GnPs and the matrix was substantially increased for the high specific surface area.²⁷ This improves the level of internal friction, slip, and dislocation motion between the GnPs and polymer chains as well as friction between GnPs.²⁸ Thus, this increased the rate of dissipating energy. This indicates that the GnPs/NBR nanocomposites are also an excellent damping material with high stiffness and loss modulus.

Underwater sound absorption properties

Figures 4 and 5 show the underwater sound absorption coefficient (α) spectra and sound pressure reflection coefficient (R) spectra of the nanocomposites at different GnPs content. The α obviously increased as the GnPs were incorporated. The optimal α of the nanocomposites was achieved as at 10 phr, and the average value of α was improved from 0.35 to 0.73—a nearly onefold increase. When the content was over 10 phr, the α of the nanocomposites decreased gradually. The trend of R with GnPs content was opposite of α with GnPs content because the relationship between α and R is $\alpha = 1 - |R|^2$.

We first introduce the sound absorption mechanisms of underwater acoustic absorbing material before explaining why the α improved significantly as GnPs were incorporated. An excellent acoustic absorbing material must meet the following two conditions^{1,3–4}: First, the impedance should match seawater so that the incident sound wave can enter into the material interior without being reflected. The impedance of a sound

medium is the product of the sound velocity in medium (c) and the density of medium (ρ). Second, the material should attenuate and disperse sound waves so that the incoming sound wave can be converted into heat energy. Once the sound waves propagate into the material interior, most of it is attenuated and dispersed by the following three main attenuation mechanisms²⁹:

The first is viscous absorption caused by the velocity gradient and viscous force between adjacent particles in the material interior. The sound viscous absorption coefficient (α_η) is given by equation (1)

$$\alpha_\eta = \frac{\omega^2}{2\rho_0 c_0^3} \left(\frac{4}{3}\eta' + \eta'' \right) \quad (1)$$

Here, ω is the angular frequency; ρ_0 and c_0 are the mass density and the speed of sound at $\omega = 0$, respectively; η' and η'' are shear viscosity coefficient and volume viscosity coefficient, respectively.

A second mechanism for the absorption is “heat conduction,” and this is described by the expression developed by Kirchhoff²⁹

$$\alpha_\chi = \frac{\omega^2 \chi}{2\rho_0 c_0^3} \left(\frac{1}{C_V} - \frac{1}{C_p} \right) \quad (2)$$

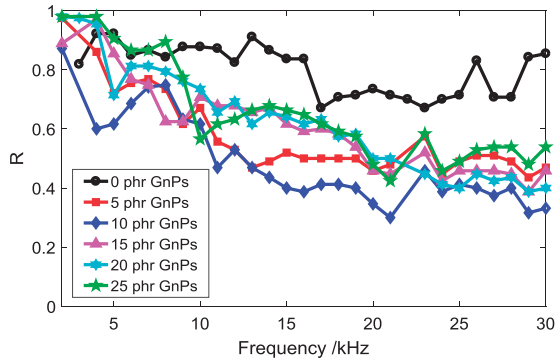


Figure 5. The sound pressure reflection coefficient spectra of nanocomposites with different GnPs contents. GnP: graphene nanoplatelet.

Here, α_χ is the sound absorption coefficient due to heat conduction, χ is the thermal conductivity, and C_V and C_p are the molecular heat capacity at constant volume and at constant pressure, respectively.

The last one is the viscoelastic relaxation mechanism caused by a large number of relaxation processes on a macromolecular level. The sound absorption coefficient α_R given by this theory is given by equation (3)

$$\alpha_R = \frac{\omega^2 c}{2c_0^2} \sum_{i=1}^n \frac{\varepsilon_i \tau_i}{1 + \omega^2 \tau_i^2} \quad (3)$$

Here, ε_i is the relaxation strength of a kind of relaxation process, and τ_i is the relaxation time.

The complex Young's modulus ($E_1 = E' + iE''$) of nanocomposites increased significantly with increasing GnPs content. This resulted in a marked improvement in the sound velocity (c) and impedance (ρc) of GnPs/NBR nanocomposites. The relationship between c and E_1 is given by equation (4)

$$c = \sqrt{\frac{E_1(1 - \nu_1)}{\rho(1 + \nu_1)(1 - 2\nu_1)}} \quad (4)$$

where ν_1 is the Poisson ratio.

As shown in Table 2, while the ρ , c , as well as ρc gradually increased with increasing GnPs content, the impedance of the GnPs/NBR nanocomposites and water ($(\rho c)_{\text{water}} = 1.45 \times 10^6 \text{ Pa}\cdot\text{s/m}$) were of the same order of magnitude. Thus, most incident sound waves could enter the nanocomposite interior with little reflection. This met the first condition of sound absorption.

Obviously, the sound wave attenuation ability of GnPs/NBR nanocomposites improved dramatically because the sound absorption coefficient α_η and α_R were improved markedly due to the notable improvements in damping properties caused by high specific surface area of GnPs. In addition, the thermal conductivity χ of nanocomposite increased due to the high thermal conductivity of GnPs (up to 5000 W/(m K)). Obviously, as more GnPs are incorporated,

Table 2. Material parameters of GnPs/NBR nanocomposites at 15°C.

Symbol	Unit	GnPs contents					
		0 phr	5 phr	10 phr	15 phr	20 phr	25 phr
ρ	kg/m ³	1198	1207	1222	1226	1235	1244
$E_1 \times 10^{-7}$	Pa	3.42 (1 + 0.74i)	6.65 (1 + 0.70i)	18.7 (1 + 0.48i)	22.7 (1 + 0.59i)	25.0 (1 + 0.45i)	44.5 (1 + 0.40i)
c	m/s	1339 (1 + 0.33i)	1851 (1 + 0.32i)	3006 (1 + 0.23i)	3347 (1 + 0.27i)	3447 (1 + 0.21i)	4561 (1 + 0.19i)
$\rho c \times 10^{-6}$	Pa. s/m	1.60	2.23	3.67	4.10	4.26	5.67

GnP: graphene nanoplatelet; NBR: butadiene–acrylonitrile rubber.

the nanocomposite has a higher χ . According to equation (2), the sound absorption coefficient due to heat conduction (α_χ) improves with increasing χ .

The incorporation of GnPs not only increased the sound wave attenuation ability but also increased the sound velocity (c). Equations (1) to (3) show that the sound absorption coefficient is inversely proportional to c . Hence, the added value of the sound absorption coefficient increased substantially when the content of GnPs was below 10 phr. It then decreased with increasing GnPs content. The improvements in η' , η'' , and χ were less than c_0^2 or c_0^3 .

Consequently, the sound absorption coefficient can be greatly improved with only 10 phr GnPs. Moreover, the mechanical properties (see below) increased, and the density was nearly unaffected. In contrast, to obtain the desired acoustic absorbing properties, it was necessary to add up to 60 phr inorganic and rigid fillers (e.g. graphite, mica powder, etc.) or porous fillers (e.g. vermiculite powder, hollow glass, aluminum microspheres, etc.) into the matrix. This sharply decreases the mechanical properties and significantly increases the density.

DSC

Figure 6 shows the influence of GnPs content on DSC of the GnPs/NBR nanocomposites and the weight of

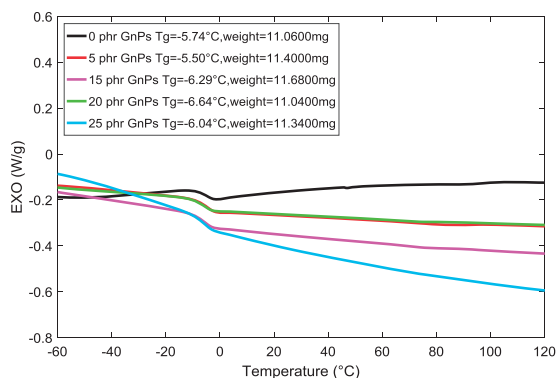


Figure 6. DSC of the GnPs/NBR nanocomposites. GnP: graphene nanoplatelet.

Table 3. The vulcanization property of the GnPs/NBR nanocomposites.

Test parameter	GnPs content					
	0 phr	5 phr	10 phr	15 phr	20 phr	25 phr
t_{10} (m:s)	1:06	1:17	1:21	1:28	1:37	1:44
t_{90} (m:s)	2:32	2:45	2:54	3:05	3:17	3:26
M_L (dN m)	0.38	0.48	0.79	1.07	1.78	2.92
M_H (dN m)	8.78	10.23	12.44	14.42	17.22	20.54

GnP: graphene nanoplatelet; NBR: butadiene–acrylonitrile rubber.

the specimens tested in DSC. The extremely mutable sites of the DSC curve correspond to the glass transition temperature (T_g) of the nanocomposite. The incorporation of GnPs does not affect the T_g , which demonstrates that the blends of GnPs and polymer matrix are thermodynamically incompatible.

Vulcanization property

Table 3 shows the influence of GnPs content on the vulcanization property of the nanocomposites. The scorch time (t_{10}) and the cure time (t_{90}) were continuously increased with increasing GnPs content. The delayed vulcanization behavior is reminiscent of the similar observations in the GO/butadiene–styrene–vinylpyridine rubber system²⁰ and GO/XNBR nanocomposites.²⁴ This is because GnPs have a large specific surface area, and the rubber accelerators can be adsorbed onto the GnPs sheets via hydrogen bonding interaction.²⁰ Meanwhile, the minimum torque (M_L) and the maximum torque (M_H) of the compound are all significantly increased with increasing GnPs content. This further suggests that the modulus of GnPs/NBR nanocomposites would be obviously improved as the GnPs were incorporated.

Mechanical properties

The mechanical properties of GnPs/NBR nanocomposites with different GnPs contents are summarized in Table 4. The tensile strength and shore A hardness were improved gradually with increasing GnPs content. When the content of GnPs was 25 phr, the tensile strength and shore A hardness increased by 35 and 29%, respectively. It seems that the reinforcing effect of GnPs was not only due to the unsatisfactory degree of dispersion of GnPs in the matrix. SEM showed aggregates of GnPs preventing the high specific surface area of GnPs from being sufficiently bonded to the matrix. The reinforcing effect of the GnPs could not be sufficiently exerted.

Table 4. The mechanical properties of the GnPs/NBR nanocomposites.

Test parameter	Unit	GnPs contents					
		0 phr	5 phr	10 phr	15 phr	20 phr	25 phr
Tensile strength	MPa	12.28	12.60	12.12	13.22	14.08	16.54
Elongation at break	%	546.17	533.46	428.35	323.01	226.75	205.91
Tear strength	kN/m	47.93	46.87	52.77	49.22	44.65	41.66
Hardness	Shore A	70	77	84	86	88	90

GnP: graphene nanoplatelet; NBR: butadiene–acrylonitrile rubber.

Table 4 shows that tear strength was increased substantially at first. It then decreased with increasing GnPs contents because the agglomeration of GnPs became more serious with increasing GnPs contents.^{30,31} The elongation at break decreased with increasing GnPs content. This might be because of a large aspect ratio and the interaction between GnPs and the matrix. This restricts the movement of the polymer chains.²³

Conclusions

We determined the dynamic mechanical properties, underwater sound absorption properties, DSC, vulcanization property, and mechanical properties of GnP-modified underwater acoustic absorbing materials. We conclude the following:

1. The E' and E'' of the NBR matrix could be significantly improved with GnPs in the matrix. This does not consider the glass transition temperature. When the GnPs content was 5 phr, the E' and E'' at 15°C improved by 94 and 84%, respectively; when the GnPs content increased to 25 phr, the E' and E'' at 15°C improved by 1201 and 603%, respectively.
2. The α increased obviously as the GnPs were incorporated. The average value of α improved from 0.35 to 0.73—an increase of nearly onefold with only 10 phr GnPs. Moreover, the mechanical properties increased, and the density remained unaffected. The merits of the GnP-modified underwater acoustic absorbing materials were higher damping, better underwater sound absorption, and better mechanical properties with unaffected density in comparison to other inorganic and rigid fillers or porous fillers.
3. The t_{10} and t_{90} were continuously increased with increasing GnPs content because the rubber accelerators can be adsorbed onto the GnPs sheets via hydrogen bonding.
4. The tensile strength and shore A hardness were improved by 35 and 29%, respectively, with 25 phr GnPs. The tear strength increased substantially at first. This then decreased with increasing GnPs content. The elongation at breaking decreased with increasing GnPs content.

Declaration of conflicting interests

The author(s) declared no potential conflicts of interest with respect to the research, authorship, and/or publication of this article.

Funding

The author(s) received no financial support for the research, authorship, and/or publication of this article.

References

1. Zhu BL and Huang XC. *Key technology of submarine acoustic stealth: design of anechoic coatings*. Shanghai: Shanghai Jiao Tong University Press, 2012.
2. Ivansson SM. Sound absorption by viscoelastic coatings with periodically distributed cavities. *J Acoust Soc Am* 2006; 119: 2558–2567.
3. Sun WH, Yan X and Zhu X. Dynamic mechanical and underwater acoustic properties of the polyurethane/epoxy resin blend elastomers filled with macroporous poly(vinyl acetate-co-triallyl isocyanurate) resin beads. *J Appl Polym Sci* 2011; 122: 2359–2367.
4. Ivansson SM. Anechoic coatings obtained from two- and three-dimensional monopole resonance diffraction gratings. *J Acoust Soc Am* 2012; 131: 2622–2637.
5. Lee CG, Wei XD, Kysar JW, et al. Measurement of the elastic properties and intrinsic strength of monolayer graphene. *Science* 2008; 321: 385–388.
6. Rao CNR, Sood AK, Voggu R, et al. Some novel attributes of graphene. *J Phys Chem Lett* 2010; 1: 572–580.
7. Balandin AA, Ghosh S, Bao WZ, et al. Superior thermal conductivity of single-layer graphene. *Nano Lett* 2008; 8: 902–907.
8. Novoselov KS, Geim AK, Morozov SV, et al. Two-dimensional gas of massless Dirac fermions in graphene. *Nature* 2005; 438: 197–200.
9. Sasha S, Dmitriy AD, Geoffrey HB, et al. Graphene-based composite materials. *Nature* 2006; 442: 282–286.
10. Kuilla T, Bhadra S, Yao D, et al. Recent advances in graphene based polymer. *Prog Polym Sci* 2010; 35: 1350–1375.
11. Chen D, Feng HB and Li JH. Graphene Oxide: preparation, functionalization, and electrochemical applications. *Chem Rev* 2012; 112: 6027–6053.
12. Georgakilas V, Otyepka M, Bourlinos AB, et al. Functionalization of graphene: covalent and non-covalent approaches, derivatives and applications. *Chem Rev* 2012; 112: 6156–6214.
13. Kuilla T, Bose S, Mishra AK, et al. Chemical functionalization of graphene and its applications. *Prog Mater Sci* 2012; 57: 1061–1105.
14. Wu ZS, Ren WC, Gao LB, et al. Synthesis of high-quality graphene with a pre-determined number of layers. *Carbon* 2009; 47: 493–499.
15. Wang GX, Shen XP, Wang B, et al. Synthesis and characterisation of hydrophilic and organophilic graphene nanosheets. *Carbon* 2009; 47: 1359–1364.
16. Kuilla T, Bose S, Khanra P, et al. A green approach for the reduction of graphene oxide by wild carrot root. *Carbon* 2012; 50: 914–921.
17. Veerapandian M, Lee MH, Krishnamoorthy K, et al. Synthesis, characterization and electrochemical properties of functionalized graphene oxide. *Carbon* 2012; 50: 4228–4238.
18. Zaman I, Kuan HC, Meng QS, et al. A facile approach to chemically modified graphene and its polymer nanocomposites. *Adv Funct Mater* 2012; 22: 32657–32875.
19. Kang HL, Zuo KH, Wang Z, et al. Using a green method to develop graphene oxide/elastomers nanocomposites

- with combination of high barrier and mechanical performance. *Compos Sci Technol* 2014; 92: 1–8.
20. Tang ZH, Wu XH, Guo BH, et al. Preparation of butadiene–styrene–vinyl pyridine rubber–graphene oxide hybrids through co-coagulation process and in situ interface tailoring. *J Mater Chem* 2012; 22: 7492–7501.
 21. Das A, Kasaliwal GR, Jurk R, et al. Rubber composites based on graphene nanoplatelets, expanded graphite, carbon nanotubes and their combination: a comparative study. *Compos Sci Technol* 2012; 72: 1961–1967.
 22. Wu JR, Huang GS, Li H, et al. Enhanced mechanical and gas barrier properties of rubber nanocomposites with surface functionalized graphene oxide at low content. *Polymer* 2013; 54: 1930–1937.
 23. Zhao X, Zhang QH and Chen DJ. Enhanced mechanical properties of graphene-based poly (vinyl alcohol) composites. *Macromolecules* 2010; 43: 2357–2363.
 24. Li YQ, Wang QH, Wang TM, et al. Preparation and tribological properties of graphene oxide/nitrile rubber nanocomposites. *J Mater Sci* 2012; 47: 730–738.
 25. Matos CF, Galembeck F, Zarbin AJG, et al. Multifunctional and environmentally friendly nanocomposites between natural rubber and graphene or graphene oxide. *Carbon* 2014; 78: 469–479.
 26. Wang JY, Jia HB, Tang YY, et al. Enhancements of the mechanical properties and thermal conductivity of carboxylated acrylonitrile butadiene rubber with the addition of graphene oxide. *J Mater Sci* 2013; 48: 1571–1577.
 27. Yuan BH, Chen M, Liu Y, et al. Damping properties of para-phenylene terephthalamide pulps modified damping materials. *J Reinf Plast Compos* 2017; 36: 137–148.
 28. Finegan IC and Gibson RF. Recent research on enhancement of damping in polymer composites. *Compos Struct* 1999; 44: 89–98.
 29. Jongen HAH, Thijssen JM, van den Aarssen M, et al. A general model for the absorption of ultrasound by biological tissues and experimental verification. *J Acoust Soc Am* 1986; 79: 535–540.
 30. Wang Y, Chen L, Yu JR, et al. Strong and conductive polybenzimidazole composites with high graphene contents. *RSC Adv* 2013; 3: 12255–12266.
 31. Zhou TN, Chen F, Tang CY, et al. The preparation of high performance and conductive poly (vinyl alcohol)/graphene nanocomposite via reducing graphite oxide with sodium hydrosulfite. *Compos Sci Technol* 2011; 71: 1266–1270.